Title

Protein-Mineral Interactions: Molecular Dynamics Simulations Capture Importance of Variations in Mineral Surface Composition and Structure.

Journal

Langmuir : the ACS journal of surfaces and colloids, 32(24)

ISSN

0743-7463

Authors

Andersen, Amity
Reardon, Patrick N
Chacon, Stephany S
et al.

Publication Date

2016-06-01

DOI

10.1021/acs.langmuir.6b01198

Peer reviewed

Protein–Mineral Interactions: Molecular Dynamics Simulations Capture Importance of Variations in Mineral Surface Composition and Structure

Amity Andersen,[*,†] Patrick N. Reardon,[†] Stephany S. Chacon,[§] Nikolla P. Qafoku,[‡] Nancy M. Washton,[†] and Markus Kleber[§,∥]

[†] Environmental Molecular Sciences Laboratory, and [‡] Energy and Environment Directorate, Pacific Northwest National Laboratory, Richland, Washington 99352, United States [§] Department of Crop and Soil Science, Oregon State University, Corvallis, Oregon 97331, United States [∥] Institut für Bodenlandschaftsforschung, Leibniz Zentrum für Agrarlandschaftsforschung (ZALF), Eberswalder Straβe 84, 15374 Mü ncheberg, Germany

*E-mail: amity.andersen@pnnl.gov.

Abstract

Molecular dynamics simulations, conventional and metadynamics, were performed to determine the interaction of model protein Gb1 over kaolinite (001), Na^+-montmorillonite (001), Ca^{2+}-montmorillonite (001), goethite (100), and Na^+-birnessite (001) mineral surfaces. Gb1, a small (56 residue) protein with a well-characterized solution-state nuclear magnetic resonance (NMR) structure and having α-helix, 4-fold β-sheet, and hydrophobic core features, is used as a model protein to study protein soil mineral interactions and gain insights on structural changes and potential degradation of protein. From our simulations, we observe little change to the hydrated Gb1 structure over the kaolinite, montmorillonite, and goethite surfaces relative to its solvated structure without these mineral surfaces present. Over the Na^+-birnessite basal surface, however, the Gb1 structure is highly disturbed as a result of interaction with this birnessite surface. Unraveling of the Gb1 β-sheet at specific turns and a partial unraveling of the α-helix is observed over birnessite, which suggests specific vulnerable residue sites for oxidation or hydrolysis possibly leading to fragmentation.

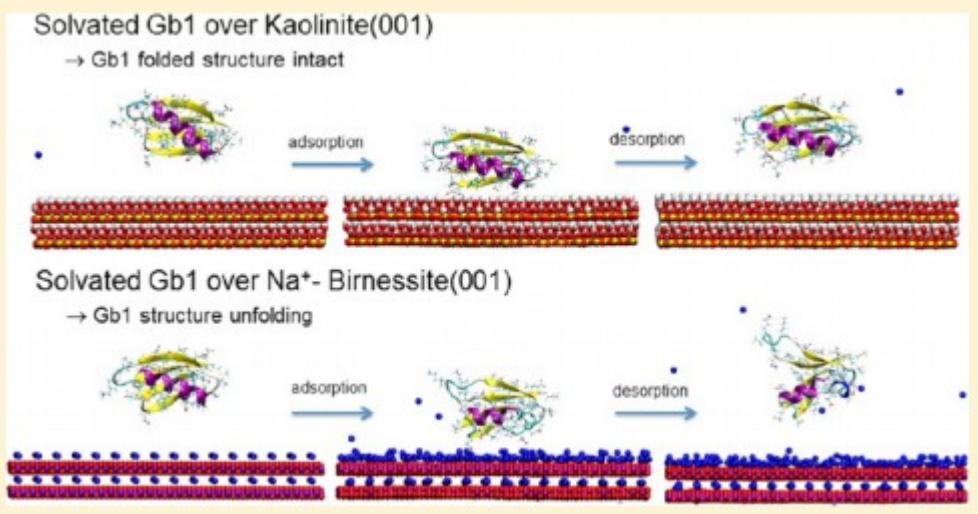

1 Introduction

Soil is the largest terrestrial source and sink of the earth's organic carbon and, therefore, has a great impact on the atmospheric carbon levels.(1-3) Not only is retention of organic carbon in soil important to climate change, it is crucial to soil quality impacting our food and fiber security.(4) A critical unknown in biogeochemical cycling, carbon biosequestration, and greenhouse gas emissions in terrestrial ecosystems is the question of mineral control over biomolecule functionality. The catabolic tools used by microorganisms for the decomposition of organic substrates are protein catalysts such as intracellular and extracellular enzymes (exoenzymes). A major factor determining the activity of extracellular enzymes is their affinity to mineral surfaces. Unfortunately, the rate-modifying capacity of mineral surfaces for enzyme activity is not a mechanistically straightforward process that may be easily predicted.(5, 6) For example, van Loosdrecht et al.(7) showed that montmorillonite may either inhibit, decrease, or increase the microbial conversion of adsorbed protein, while Russo et al.(8) were able to demonstrate that manganese oxide may induce the disappearance of prion protein from soils at low pH. Hence, the question arises: How do abiotic, geochemical factors such as mineral surface characteristics contribute to, induce, or modify the functionality of enzymatic tools?

Experimental studies of the interaction of biological and natural organic matter (NOM) with mineral surfaces, involving multiple techniques, such as nuclear magnetic resonance (NMR), X-ray diffraction (XRD), Fourier transform infrared spectroscopy (FTIR), Raman, atomic force microscopy (AFM), and ultraviolet and visible spectroscopy (UV/vis), have been performed in the realms of soil science,(5, 6, 9-20) biotechnology,(16, 21-23) agricultural technology,(24) food processing,(25-27) water treatment,(28) and many industrial processes.(17, 29, 30) These studies have been concerned with the chemical and structural stability of biological or organic matter on mineral surfaces. For protein–mineral interactions in these realms, preservation of the enzymatic activity of the adsorbed or immobilized protein is also of interest. Phyllosilicate (e.g., smectite and kaolinite) mineral interactions with biomolecules and organic molecules have been of primary interest in many of these experimental studies.

From an atomistic viewpoint, molecular dynamics simulations can be employed to gain insight into soil organic carbon (SOC)–mineral surface interactions where experimental observation and measurement may be difficult to perform or interpret. To the best of our knowledge, molecular dynamics has only been used to study NOM-mineral interactions for a few instances. It has been applied to study NOM-mineral interactions using NOM model molecules possessing many of the chemical and physical properties of NOM.(31-34) Molecular dynamics was also applied to nucleic acid (e.g., DNA, RNA, ribosomes)–mineral interactions pertinent to the solving of the origins of life mystery.(35-39) The interactions of protein (e.g., hen egg white lysozyme,(40, 41) fibronectin(42)) with silica in the context of

biotechnological applications (e.g., drug/nutrient delivery) were also determined with computer simulations. The former two series of studies focused on phyllosilicate surfaces, primarily smectites such as montmorillonite. The latter series of studies involves charged silica or mica mineral surfaces. We are aware of only one study of protein (i.e., lipase) interacting with a transition metal oxide (TMO) surface (rutile TiO_2(110)).(43) TMO minerals can be involved in redox (electron-transfer) reactions leading to potential catalytic change, denaturing, and decomposition of SOC in different soil systems. The interaction of SOC or biological matter with soil-relevant TMO minerals such as Fe oxides (hydroxides) and Mn oxides (hydrates and hydroxides) has not been studied with molecular simulation methods. Moreover, a comparison of protein interactions with multiple types of realistic hydrophilic mineral surfaces present in soil has not been explored atomistically using molecular dynamics simulations.

In this work, and for the first time to the best of our knowledge, molecular dynamics simulations are used to study the structural changes of the well-characterized (via solution-state NMR(44) and crystallography(45)) and remarkably stable (reversible melting at 87 °C)(44) β1 immunoglobulin-binding domain of streptococcus protein G (i.e., Gb1) interacting with kaolinite, montmorillonite, goethite, and birnessite surfaces. The aim of our work is to provide insight into the potential stabilization or destabilization mechanisms of soil proteins, with various mineral surfaces present in soil. As protein-mineral interactions are of overriding importance for decomposition processes in complex soil systems, this insight can be considered vital to achieve the goal of including decomposer functionality into decomposition models.(46) In addition, this work sheds light on potential changes in protein (e.g., microbial or plant root exudate extracellular enzymes) activity as a result of mineral surface interactions, which impacts the SOC microbial decomposition rates.

2 Theoretical Approach

2.1 Mineral Surfaces, Protein Model, and Force-Field Parameters

Each of the four mineral bulk lattice models (kaolinite, montmorillinite, goethite, and birnessite) were constructed using the crystallography data from Bish et al.(47, 48) for kaolinite, Viani et al.(49) for montmorillonite (Na^+ and Ca^{2+}), Yang et al.(50) for goethite, and Lopano et al.(51) for triclininc Na^+-birnessite. For the montmorillonite, nonadjacent, central alumimum atoms were substituted with Mg^{2+}, and silicon atoms were replaced with Al^{3+} (Wyoming-type) to give a supercell with the stoichiometry: $H_{128}Na_{24}Mg_{16}Al_{120}Si_{248}O_{768}$ for the Na^+-montmorillonite and $H_{128}Ca_{12}Mg_{16}Al_{120}Si_{248}O_{768}$ for the Ca^{2+}-montmorillonite. Water molecules (not included in the crystallographic data of Viani et al.(49)) were loaded into the montmorillonite interstitial spaces using Gibbs ensemble Monte Carlo (GEMC) simulations with constant temperature (300 K) and pressure (1 atm) via the Towhee program.(36) The CLAYFF force-field potential parameters of Cygan

et al.(52) for the montmorillonite lattice and the SPC/E force-field potential parameters of Berendsen et al.(53) for the water molecules were used in the GEMC simulations. For the birnessite system, the lattice was expanded to a 1 × 2 × 1 supercell with one sodium cation in the interstitial. Three water molecules were placed around the sodium cation in the interstitial to give an idealized composition of $NaMn_4O_8 \cdot 3H_2O$ (Figure 1). Surface models were cleaved from these initial bulk lattice models using the Materials Studio software.(54) The resulting planes of interest in this work are the kaolinite (001), montmorillonite (001), goethite (100), and birnessite (001) surfaces (Figure 2). Surface charge density for charged mineral systems (MMT and birnessite) or active site number density for uncharged mineral systems (kaolinite and goethite) can be found in the Supporting Information (Table S2).

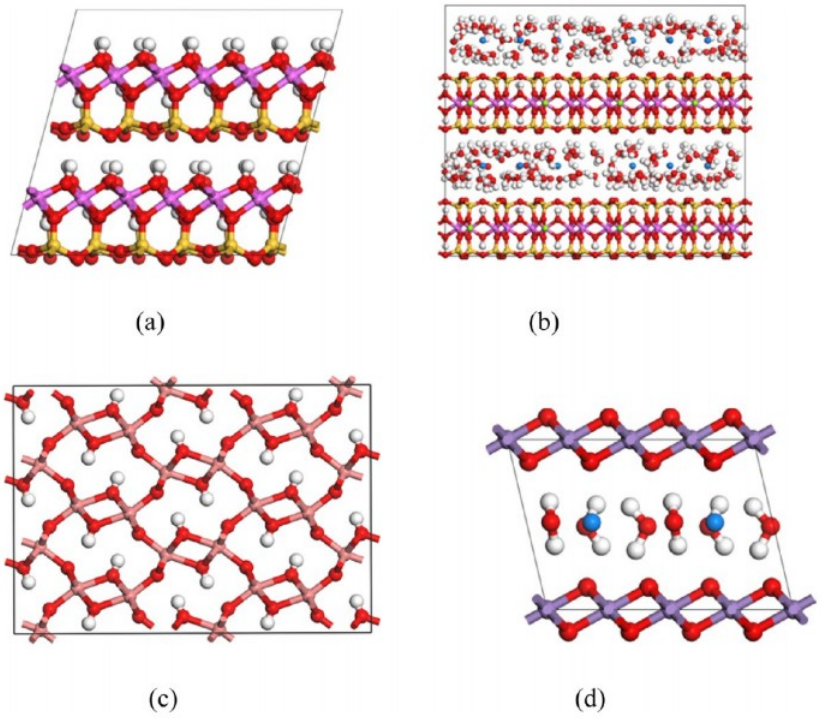

Figure 1. Atomistic lattice models of the mineral systems of interest: (a) kaolinite, (b) Na^+ or Ca^{2+} montmorillonite (MMT), (c) goethite, and (d) Na^+ birnessite. (Color scheme: white, H; red, O; magenta, Al; gold, Si; green, Mg; blue, Na; cyan, Ca; pink, Fe; purple, Mn.)

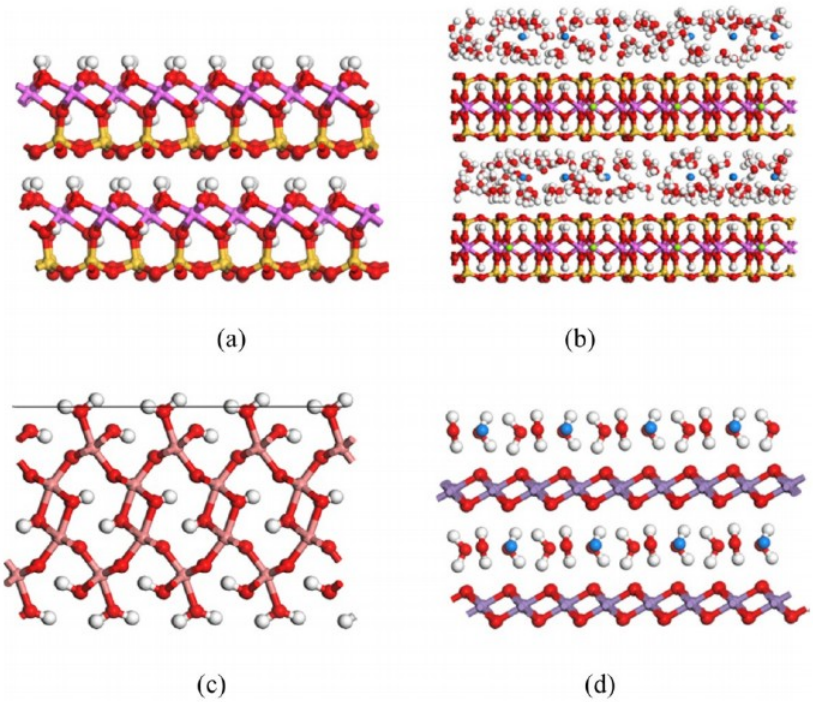

Figure 2. Mineral surfaces considered in this work: (a) kaolinite (001), (b) montmorillonite (001), (c) goethite (100), and (d) birnessite (001).

To accommodate large protein structures, these surfaces were expanded in the xy plane to between 72 and 92 Å in the x direction and between 71 and 92 Å in the y direction with an aim of achieving similar surface areas. For the kaolinite surface, the resulting surface was a two-layered 82.384 × 80.406 Å surface. For both the Na^{+} and Ca^{2+}-montmorillonite surface, the resulting surfaces were two-layered 82.880 × 71.840 Å dimensional surfaces. For the goethite (100) surface, an 81.481 × 82.762 Å surface was created. For the birnessite system, the resulting two-layered system had the dimensions 82.194 × 91.123 Å. After extending the surfaces, a 100 Å vacuum layer was placed on top of the each surface. Periodic boundary conditions are assumed for these models.

The pdb file for the Gb1 protein structure was obtained from the Protein Data Bank (pdb code 1Gb1 from http://www.rcsb.org/pdb/home/home.do) (Figure 3). The protein structure was placed over each of the five surface models, giving an ~10 Å distance between the bottom of the protein and the surface. The protein was initially oriented with the Gb1 electric dipole roughly parallel to the surface normal. This initial orientation is in line with the preferred orientation of Gb1 over self-assembled monolayers (SAMs) with a surface termination of positively charged ammonium groups as determined by the MD simulations of Liu et al.(55) Though not expected to be the preferred orientation of Gb1 over the surfaces of interest in this study, model cells were also constructed with the Gb1 electric dipole antiparallel to the surface normal. The vacuum around the protein and above the surface in each of the five cases was randomly filled with water molecules using the Packmol program(56) to a 1 g/cm^3 density for the water-molecule-occupied volume of

the system box. Four Na^{+} atoms for all systems except for that of Ca^{2+}-MMT (two Ca^{2+} atoms instead) were used to balance the net $4e^{-}$ charge of the Gb1 protein above its IEP pH. Variation of ionic strength of the aqueous phase will be considered in future work. The resulting pdb files were then used as input in the home-grown Python program to generate LAMMPS(57) data files containing the system topologies and properly assigned force-field parameters. The AMBER (ff99SB) force-field(58) was applied to the protein system, the CLAYFF force-field (with the Mn^{3+} and Mn^{4+} extensions of Andersen(59) and the reparameterization of the Fe^{3+} potential developed by Kerisit(60)) were applied to the mineral surfaces and solvated counterions, and the SPC/E force-field was applied to the water molecules. The pH of all the simulations was a neutral 7 pH.

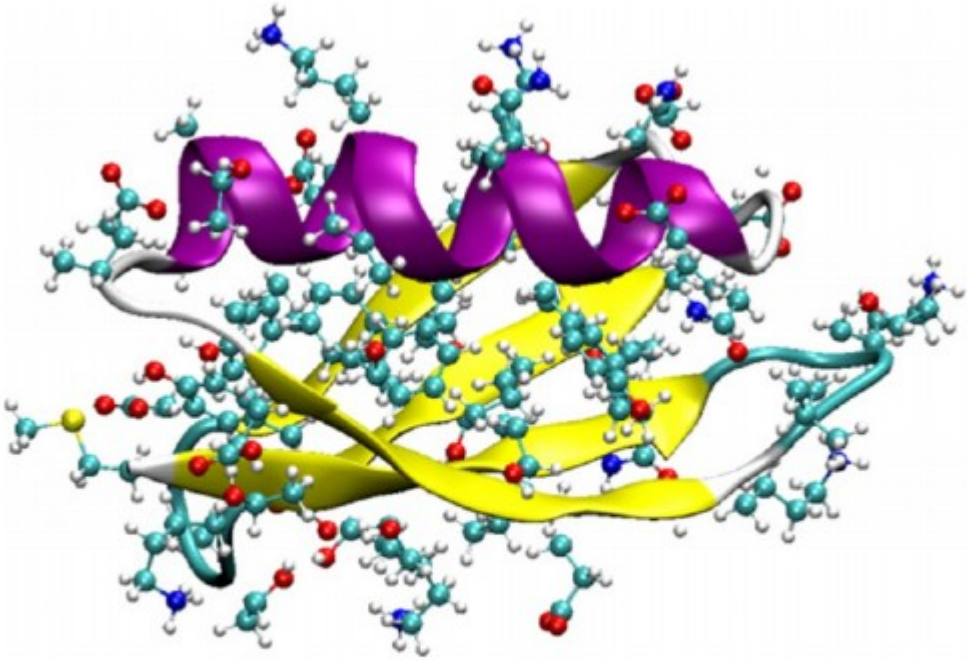

Figure 3. Gb1 protein. Purple ribbon represents α-helix secondary structure, and yellow arrows represent 4-fold β-sheet secondary structure. The CPK balls represent side groups: blue-green, C; red, O; blue, N; white, H; yellow, methionine S.

2.2 Molecular Dynamics Simulations

After the LAMMPS data files were generated, conventional molecular dynamics (MD) simulations were performed. All MD simulations were performed with the LAMMPS massively parallel MD program.(57) The particle–particle particle-mesh (PPPM) method was used to calculate the long-range electrostatic interactions. The generated models were first minimized using the conjugate-gradient method. After minimization, each system was thermalized with a ramp up in temperature from 50 to 300 K over 1 ns at NVT. Following this initial thermalization, each system was

equilibrated at 300 K with NPT (for 1 ns). Finally, each system was run for a simulation time duration of 80 ns. The SHAKE algorithm was applied to keep all H-bearing bonds and the bond angles of the water molecules fixed. This allowed for a longer 2 fs time step. After the completion of the MD simulations, the trajectories were visualized and analyzed using the VMD software package.(61) Details of the analyses used can be found in the Supporting Information (section 3).

Following conventional MD simulations, further metadynamics simulations were performed to determine the free energy of the protein binding to the mineral surfaces and to accelerate the sampling of configurations that may not be readily observed with relatively short conventional MD trajectories. This was performed using the COLVARS(62) package interfaced to the LAMMPS molecular dynamics program. The metadynamics simulations probed one collective variable, the center of mass distance between the surface and Gb1. The hill height and width of the added Gaussians were set to 0.01 kcal/mol and 0.25 Å, respectively. The Gaussians were added every 1000 ps. The durations of metadynamics simulations were 502.9, 621.9, 479.4, 677.4, and 501.1 ns for kaolinite (001), Na^+-MMT(001), Ca^{2+}-MMT(001), goethite (100), and Na^+-birnessite(001), respectively.

3 Results and Discussion

3.1 Solvated Gb1-Kaolinite (001) Complex

First, we present our results of the Gb1–kaolinite interactions. Kaolinite is a phyllosilicate mineral having a layered structure. A layer of kaolinite is polar in the direction normal to the (001) basal surface with one side covered with protons at bridging oxygen sites attached to a gibbsite-like aluminum layer, and the other side of the layer is terminated by bridging oxygen ions attached to a tetrahedral silicon layer. Unlike montmorillonite, kaolinite is a nonswelling clay (i.e., water or other molecules/ions penetration into the interlayer space to cause expansion of the interlayer is unfavorable). With Gb1's overall negative charge (−4e) at pH 7, the protein is more likely to adsorb on the alumina side basal plane of kaolinite (IEP between 6 and 8(63)) with its negatively charged carboxylate side groups, carboxylate terminus, and neutral electronegative polar groups. Our simulations reveal binding mechanisms that are consistent with this hypothesis (Figure 4). Water molecules also strongly interact with the hydrophilic surface and compete with the protein adsorption, which is the reason for the gap in contact between the Gb1 protein and kaolinite surface. This has been shown in other MD simulation studies involving proteins over hydrophilic surfaces (i.e., silica, TiO_2, SAMs).(40, 43, 64, 65) Experimentally, FT-IR data indicate the absence of hydrogen bonds between the proteins (i.e., whey proteins, α-lactalbumin, bovine serum albumin, β-lactoglobulin) and kaolinite surfaces. (25, 26)

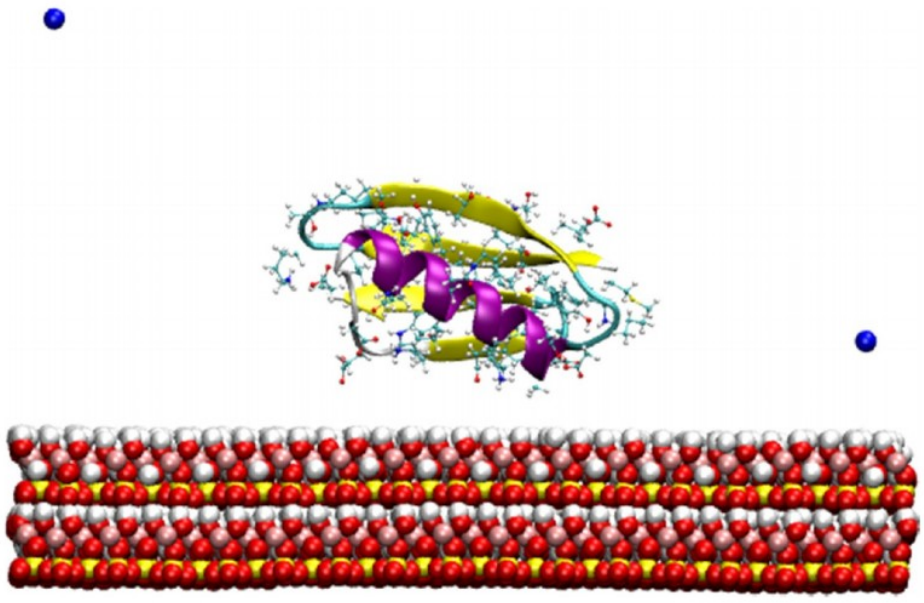

Figure 4. Gb1 adsorbed to kaolinite proton-covered (001) basal surface. Simulation snapshot (80 ns) with water molecules removed for clarity.

3.2 Solvated Gb1-Na^+/Ca^{2+}-Montmorillonite (001) Complex

Like kaolinite, montmorillonite (MMT) is a phyllosilicate mineral. However, montmorillonite has a 2:1 structure with an octahedral aluminum oxide layer sandwiched between two tetrahedral silicon oxide layers. Both sides of a layer are terminated by bridging oxygen ions. This is not a polar arrangement of atoms like the kaolinite layers. Moreover, the Wyoming-type MMT can have tetrahedral aluminum substitutions of silicon at the tetrahedral silicon outer layers of a MMT layer to create a net negative charge in addition to those substitutions in the octahedral aluminum layer. The net negative charge is balanced by the presence of alkali or alkaline earth metals (e.g., Na^+, Ca^{2+}) in the interlayers accompanied by water molecules. However, unlike kaolinite, MMT has a greater swelling potential (i.e., addition of water or other molecules that expand the interlayer).

Though the aluminosilicate layers are negatively charged, the negatively charged Gb1's carboxylate and nonpolar electronegative groups can interact with the charge-balancing cations present at the surface (unless the cations diffuse away from the surface through the aqueous solution). Our simulations show that the ammonium cation groups of the protein, however, are attracted to the negatively charged MMT layers. Compared to the Gb1-kaolinite (001) system, Gb1 seems to have minimal contact with the MMT (001) basal surface (Figure 5). Consistent with this result, Ca^{2+}-MMT has been shown by Naidja et al. not to immobilize protein tyrosinase, which, like Gb1, carries a net negative charge at pH 7; however, MMT coated with Al hydroxide (comparable to the gibbsite side of kaolinite) readily immobilizes tyrosinase. The immobilized tyrosinase was less sensitive to temperature and retained activity longer compared to free tyrosinase.(14) "Soft" (i.e., flexible) protein bovine serum albumin (BSA) (IEP 4.8) adsorbs, intercalates,

and denatures in/on Na^+-MMT.(17, 66) However, Ca^{2+}, unlike Na^+, does not stabilize the adsorption of BSA.(17) Interestingly, “hard” (i.e., rigid) protein hen egg white lysozyme (HEWL; IEP 11) adsorption is stabilized by Ca^{2+} on MMT and is not denatured.(17) This could be due to the net positive charge of HEWL, which would be more electrostatically attractive to the negatively charged MMT compared to Gb1 or tyrosinase.

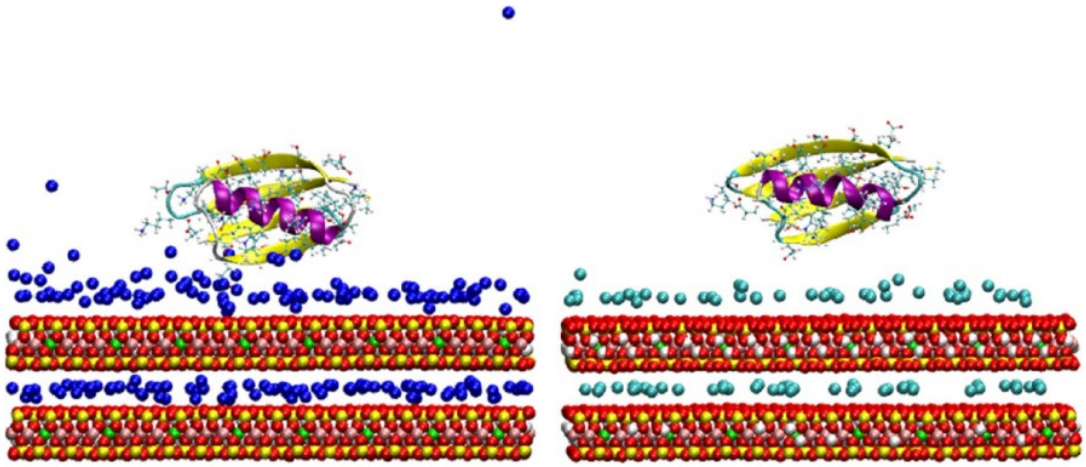

Figure 5. Gb1 adsorbed to Na^+-MMT(001) (left) and Ca^{2+}-MMT(001) (right) basal plane. Simulation snapshot (80 ns) with water molecules removed for clarity. Compared to the Gb1-kaolinite case, a single carboxylate group is interacting with the surface via a Na^+ cation (in blue) after 80 ns of simulation. For the Ca^{2+}-MMT(001) case, Gb1 is not interacting substantially with Ca^{2+} (in cyan) covered surface.

The MMT (010) edge surface is believed to be a more chemically reactive surface than the basal surface as it has more hydroxyl groups that can participate in acid/base chemistry. Moreover, the hydrated interlayers may be able to incorporate the cationic ammonium groups of the protein leading to enhanced adsorption of the protein, and intercalation or partial intercalation is possible. However, in contrast to the highly positive “hard” globular protein HEWL with a high IEP of 11.4, which has been observed to readily intercalate smectite saponite,(22) the net negative charge ($-4e^-$) of “hard” protein Gb1 at pH 7 makes it unlikely to readily intercalate smectites. Finally, regarding NOM adsorbed on MMT, Chorover et al. observed no shift of carboxylate peak in their diffuse reflectance infrared Fourier transform (DRIFT) spectra, though carboxylate uptake by MMT was apparent, indicating a possible cation or water bridging mechanism.(19)

3.3 Solvated Gb1-Goethite (100) Complex

Next, we looked at Gb1 on goethite. Goethite is known via scanning transmission X-ray microscopy (STXM) to bind protein-rich domains of extracellular polymeric substances (EPS)(9) and bind acid phosphatase (with some structural distortion as indicated by a broad blue-shifted amide I band in the FTIR).(10) Goethite has an elongated crystal morphology with (010), (110), (100), and (021) crystal faces.(67) As a first simulation with the goethite system, we chose the (100) surface.

The (100) surface is a corrugated surface with depressed bridging hydroxyls hydrogen-bonding within the surface structure and outer water ligands

chemisorbed to the iron cations. The overall charge of the (100) surface slab system is neutral; however, the surface can be considered to be zwitterionic, terminated by hydroxyls and Fe^{3+} ions with labile chemisorbed water ligands; carboxylate groups from the Gb1 could feasibly displace the water ligands and interact with the Fe^{3+} cations. The carboxylate groups of Gb1 can also interact with the water ligand protons, and the cationic Na^{+} and ammonium groups can interact with the bridging hydroxyl oxygen atoms. In the simulations, Gb1 interacts with the goethite (100) surface minimally with a single carboxylate (Figure 6). The goethite (100) surface appears to be one of the least disturbing surfaces for Gb1. However, Chorover and Amistadi's DRIFT analysis of NOM (in which proteins and peptides are a subset) indicates that Fe-carboxylate complexes may form on the goethite surface. (19) We will explore this further in our discussion of the metadynamics simulations.

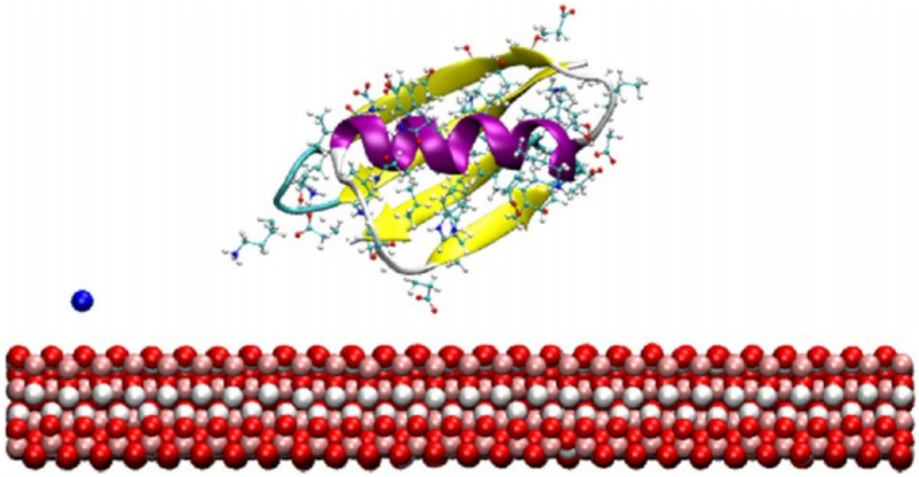

Figure 6. Gb1 adsorbed to the goethite (100) plane. Simulation snapshot (80 ns) with water molecules removed for clarity.

3.4 Solvated Gb1-Na^{+}-Birnessite (001) Complex

In the simulations of solvated Gb1 on top of the (001) basal surface of birnessite covered with charge-neutralizing Na^{+}, we find that the structure of Gb1 is highly disrupted by the Na^{+}-birnessite surface. After 40 ns of simulation time, we find that the structure of Gb1 shows signs of unfolding (Figure 7). The carboxylate groups of the protein are attracted to the Na^{+}, which is a highly dense charged layer closely held by the birnessite (001) surface. Compared to the Gb1-Na^{+}/Ca^{2+}-MMT basal systems, the layer of counter-cations is much less diffuse in the *z*-direction normal to the surface. It is possible that the high surface charge density and structure of water at the surface is disruptive to the hydrogen bond network of protein in the Na^{+}-birnessite case.

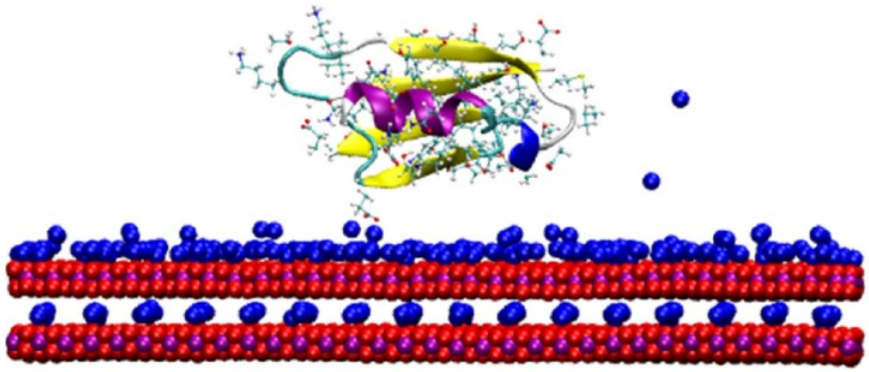

Figure 7. Gb1 adsorbed to Na^+-birnessite (001) basal plane. Simulation snapshot (80 ns) with water molecules removed for clarity. After 80 ns of simulation, Gb1 shows loss of the folded structure in the α-helix and β-sheet (see top left turn in figure).

For tyrosinase–birnessite and bovine serum albumin (BSA)–birnessite complexes, Naidja et al. observed with atomic force microscopy (AFM) that the immobilized tyrosinase and BSA structures showed unfolding and flattening, and their FTIR spectra revealed a weakening of the amide I and II modes of the polypeptide chains of these two proteins, indicating a possible loss in the proportion of α-helix.(20) We also see evidence for similar structure deformation of Gb1 over birnessite in our simulations. Unraveling of the protein structure could open functional groups such as the amide backbone bonds to catalytic reaction such as hydrolysis and oxidation, leading to possible fragmentation over the highly reactive manganese oxide surface. This may be catalyzed by hydrated out-of-plane Mn^{3+} species in a low pH environment in the case of low Mn vacancy birnessite.(68) As with MMT, the edge surface of birnessite is likely to be more reactive than the basal surface. In the case of high Mn vacancy birnessite, such as "*c*-disordered" H^+-birnessite,(69) vacancy sites are comparable to oxygen edge sites with a high proton affinity and could participate in acid-catalyzed hydrolysis reactions. Interestingly, Chorover and Amistadi's DRIFT spectra indicate that NOM may not be retained as strongly by birnessite as it is for goethite, but have noted birnessite's higher chemical reactivity as indicated by the production of hydroxide and aliphatic acids.(19)

3.5 Comparing the Influence of the Mineral Surfaces on the Solvated Gb1 Protein

3.5.1 Gb1 Structure, Orientation, Dipole Moment

For the orientation of the molecule, we compare the dipole and dipole moment of the Gb1 over the five mineral surfaces. Figure 8 below depicts the Gb1 dipole with relative magnitude over the five mineral surfaces. As shown by the MD simulation work of Kubiak-Ossowska and Mulheran(40) with hen egg white lysozyme (HEWL) over a charged silica surface and by Liu et al.(55) with Gb1 over charged self-assembled monolayers (SAM), molecular dynamics simulations of protein adsorption are driven, to a major extent by electrostatics. The direction of the protein dipole guides the orientation and motion of the protein. We see that Gb1 over the Na^+-birnessite (001) surface

has the most surface-normal aligned dipole with the largest magnitude of the five mineral complexes. The large dipole moment is a result of the disruption in folded structure and the flattening of Gb1 over the Na^+-birnessite (001) surface. The dipole of Gb1 over Na^+-MMT(001), Ca^{2+}-MMT(001), and goethite (100) shows wider angles with the surface normal. With Gb1 over kaolinite (001), the dipole is closer to being parallel with the surface compared to that of the other four surface complexes. The tilt is due to increased interaction of multiple carboxylate functional groups with the proton-covered surface.

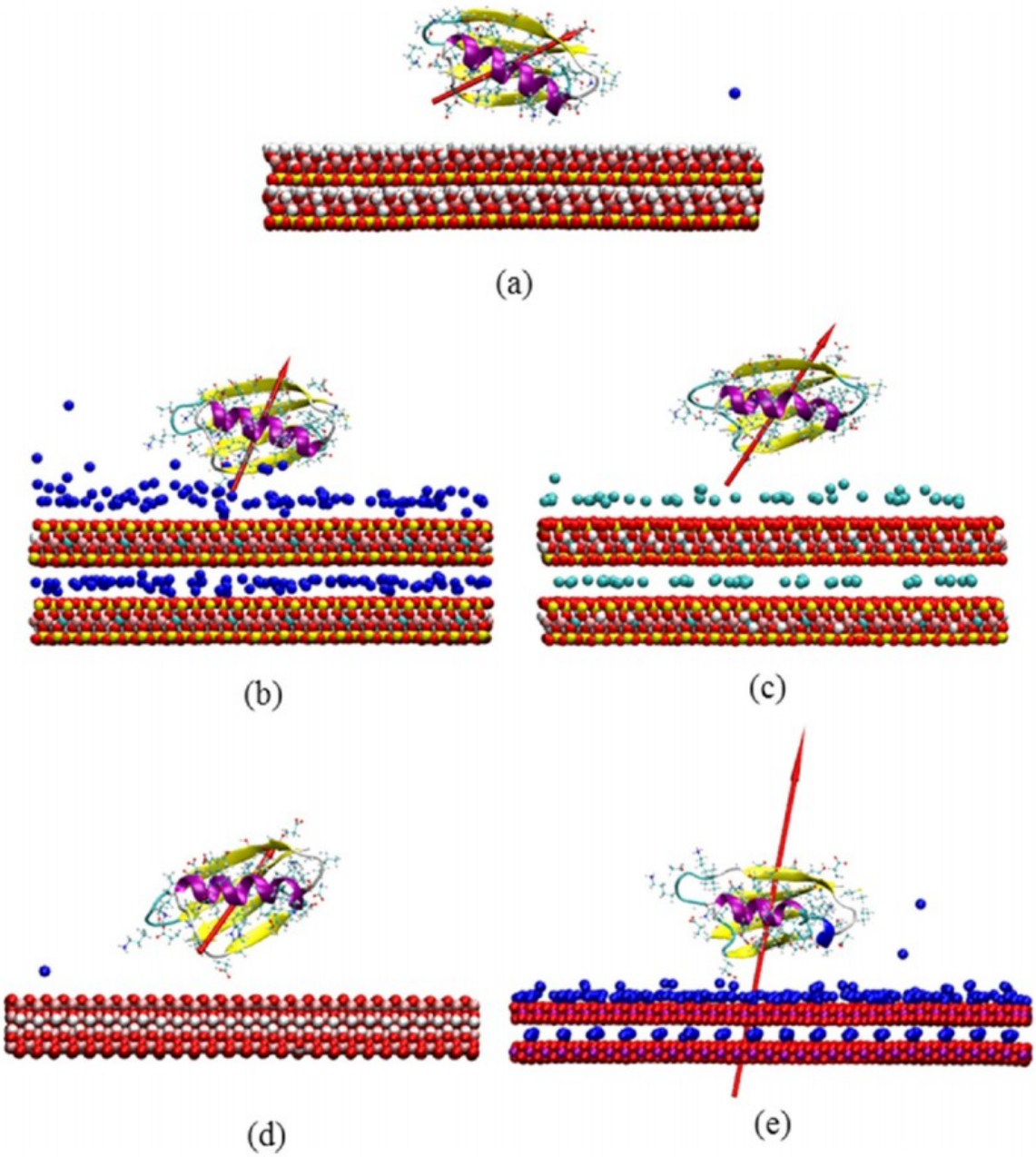

Figure 8. Gb1 dipole orientation and relative magnitude (represented by red arrow) over the five surfaces after 80 ns of simulation time. (a) Gb1-kaolinite (001), (b) Gb1-Na^+-MMT(001), (c) Gb1-Ca^{2+}-MMT(001), (d) Gb1-goethite (100), and (e) Gb1-Na^+-birnessite (001).

From recent molecular dynamics work of Liu et al. with Gb1 over charged SAMs, Gb1s tended to adsorb on the aminated (positively charged) SAM surface with the dipole in the direction of the surface normal, with an acute angle to the surface normal.(55) We see a similar tendency for Gb1 to dock on the complex hydrophilic mineral surfaces having positive surface charges such as Na^+ (MMT, birnessite), Ca^{2+} (MMT), and protons (kaolinite) with the dipole pointed in the direction of the surface normal. However, this tendency is less pronounced for polar, but neutral, kaolinite (001) and neutral, zwitterionic, goethite(100). For kaolinite(001), the attraction of negatively charged aspartate and glutamate (especially GLU42) side groups tends to tilt the angle of the dipole with respect to the surface normal more toward being parallel to the surface. In the case of goethite (100), the positive lysine side groups are also attracted to the hydroxyl group oxygen atoms with buried protons. This can direct the end with LYS10 and LYS13 toward the goethite surface, tilting the Gb1 dipole to be more parallel with the surface normal. With the depletion of mobile cations Na^+ and Ca^{2+} from the MMT and birnessite surface through diffusion, we should see further tilting of LYS10 and LYS13 toward the negatively charged base MMT and birnessite oxide layers. Tilting would be more pronounced for the MMT systems compared to the birnessite system due to birnessite's tendency to retain Na^+ cations at the surface).

In Figure 9, we show the evolution of the dipole moment over the simulation time. The changes in the dipole moment with simulation time roughly reflect the changes in structure we have shown with the root mean squared deviation (RMSD) comparison. The Na^+-birnessite system brings about the highest magnitude change in the Gb1 dipole moment. Importantly, the Ca^{2+} and Na^+ MMT (001) surface complexes initially show a fairly high Gb1 dipole moment, but the value of these dipole moments taper down to a dipole moment that is close to that of the solvated Gb1 with no surface. In the case of the Ca^{2+}-MMT (001) this taper appears to be more gradual compared to that of Na^{+}-MMT (001).

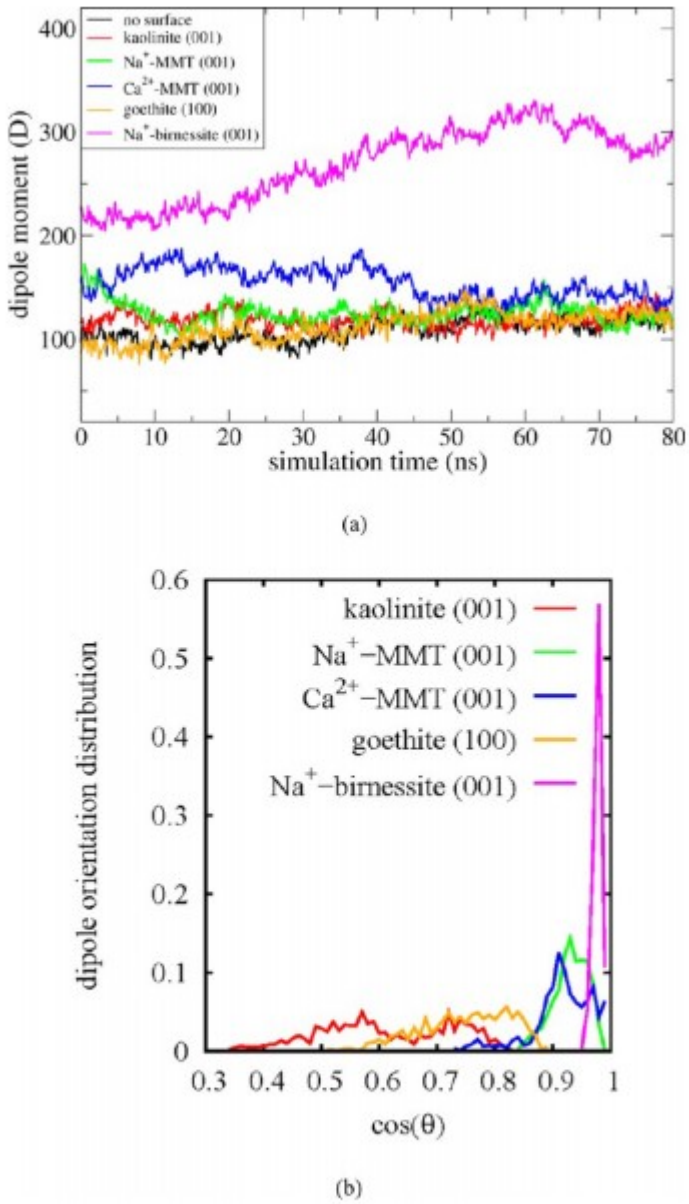

Figure 9. (a) Gb1 dipole moment over five mineral surfaces and without a surface present as a function of simulation time. (b) Gb1 dipole orientation distributions over five mineral surfaces.

Comparing the RMSD from the initial Gb1 structure as a function of time (Figure 10) for the surfaces considered, we observe that Na^+-MMT basal surface preserves the structure of Gb1 the best (i.e., the RMSD from the solution NMR-determined structure is the least). Interestingly, the Na^+-MMT basal surface stabilizes a Gb1 structure closest to the solution-phase NMR determined structure, even when compared with the water-solvated Gb1 with no mineral surface present. This may be due to the high ionic strength at the Na^+-MMT basal surface imparted by the high concentration Na^+ cation layer at the surface, which is broad enough to encompass the Gb1 protein

(unlike the case of the Na^+-birnessite system where the cations are tightly held by the birnessite surface). The goethite (100) surface disturbs the Gb1 structure slightly more than the Na^+-MMT basal surface. Goethite (100) has a combination of hydroxyl and Fe^{3+} cations terminating the surface with labile water ligands above. The protein competes with water molecules for the surface reactive sites, and the simulations do not show significant interaction of charged groups, carboxylates and ammoniums; only a single carboxylate group from GLU42 interacts with the surface. MMT with divalent Ca^{2+} disturbs the Gb1 structure slightly more than the monovalent Na^+-MMT basal surface; this is possibly due to divalent Ca^{2+} staying closer to the surface and not desorbing as readily as monovalent Na^+, which creates a thicker layer of cations. The kaolinite basal surface, with a covalently bound layer of protons at the aluminum side, has an intermediate impact on the structure, but the folded Gb1 is intact. The Gb1 over birnessite shows the most change, and, as we show in Figure 7, the Gb1 folded structure is beginning to unravel at locations in the β-sheet and in the α-helix after 80 ns. The Gb1 structure also appears to be more compressed over the Na^+-birnessite basal surface as indicated by the relatively small eccentricity reported in Table 1.

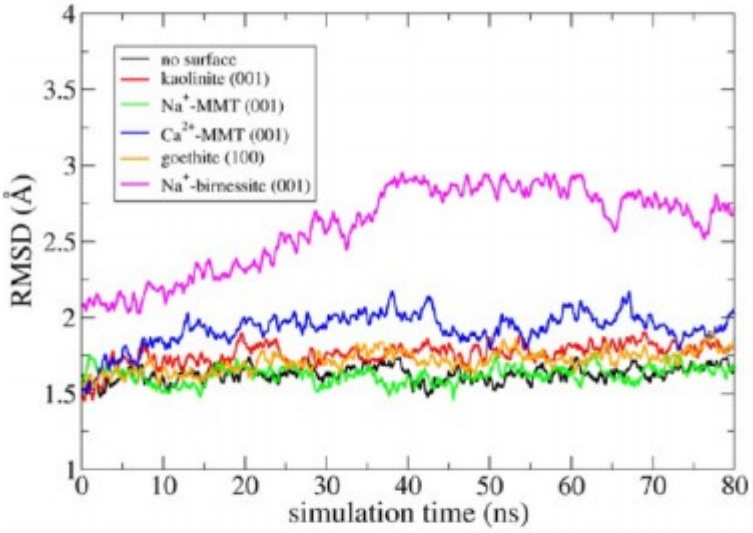

(a)

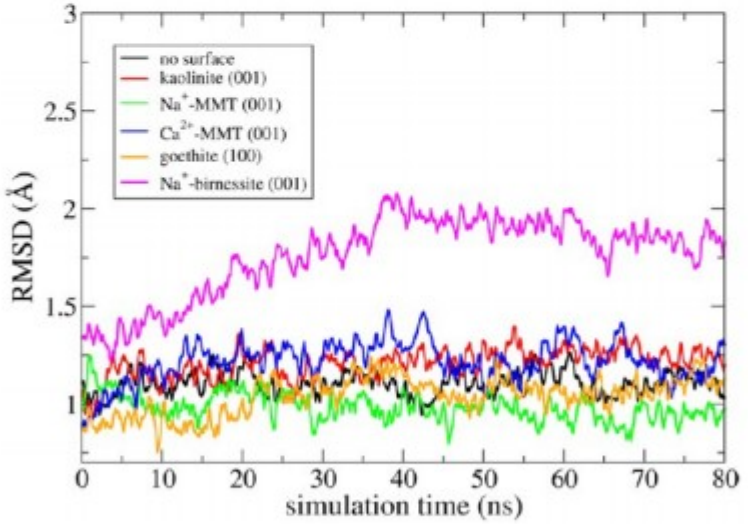

(b)

Figure 10. (a) All-atom RMSD of Gb1 structure from the starting structure from the protein database for the different mineral interactions, starting from 0 ns after equilibration. (b) Backbone RMSD of Gb1 structure.

Table 1. Averages and Standard Deviations over 80 ns for the Dipole Moment, Dipole Orientation with Respect to the Surface Norm, RMSD, Radius of Gyration (R_g), and Eccentricity for Solvated Gb1 Interacting with the Five Mineral Surfaces and Solvated Gb1 with No Surface

surface	dipole moment (D)	dipole orientation ($\cos(\theta)$)	average dipole orientation (deg)	RMSD (Å)	R_g (Å)	eccentricity
no surface	108 ± 11			1.63 ± 0.05	10.84 ± 0.05	0.197 ± 0.003
kaolinite (001)	119 ± 8	0.62 ± 0.11	52	1.76 ± 0.07	10.76 ± 0.04	0.196 ± 0.004
Na^+-MMT (001)	125 ± 11	0.94 ± 0.03	21	1.62 ± 0.06	10.76 ± 0.04	0.196 ± 0.003
Ca^{2+}-MMT (001)	155 ± 15	0.92 ± 0.05	23	1.93 ± 0.11	10.99 ± 0.05	0.204 ± 0.004
goethite (100)	112 ± 14	0.75 ± 0.08	41	1.71 ± 0.07	10.80 ± 0.08	0.196 ± 0.006
Na^+-birnessite (001)	268 ± 35	0.98 ± 0.01	11	2.60 ± 0.28	11.04 ± 0.07	0.184 ± 0.006

Figure 11 shows the heat maps for the RMSD for each Gb1 residue as a function of time. Gb1 over Na^+-birnessite shows the most RMSD for the ammonium-side chain lysine residues LYS10 and LYS28 and ASP36. LYS10 is part the first β-sheet turn showing the most structural change, and this is reflected in the adjacent residues of the heat map in Figure 11. LYS28 is in the middle of the α-helix. ASP36 is toward the end of the α-helix furthest away from the surface. Ca^{2+}-MMT also shows a similar, yet less pronounced, pattern with LYS10 and LYS28. LYS50, part of the last β-sheet turn, also shows some change over Ca^{2+}-MMT. Table 1 summarizes the averages and standard deviations of the dipole moment, dipole orientation with respect to the surface norm, RMSD, radius of gyration (R_g), and eccentricity for Gb1 interacting with the five mineral surfaces and solvated Gb1 alone over the 80 ns simulation.

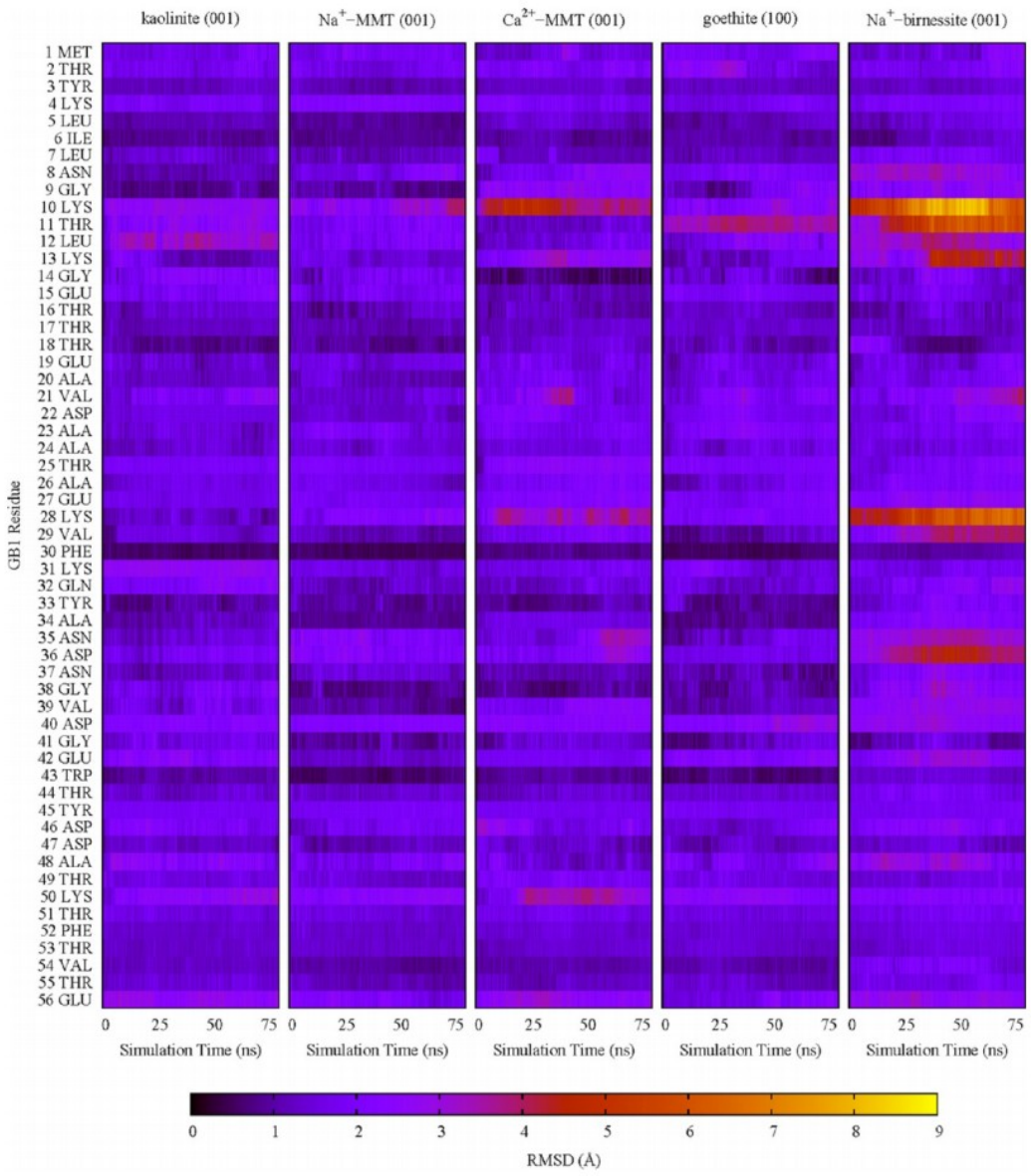

Figure 11. Heat map of all-atom RMSD for each Gb1 residue as a function of simulation time.

3.5.2 Water Structure of Solvated Gb1 Mineral Complexes

Comparing the hydrogen-bonding of the water molecules for the five Gb1 mineral complex systems, the Gb1-goethite (100) complex system, after 80 ns, shows the most hydrogen-bonds per water molecule followed by the Gb1-kaolinite (001) surface complex (see Figure 12). It appears that the Gb1-goethite (100) complex enhance the hydrogen-bonding of water compared to the solvated Gb1 system without a mineral surface. The Gb1-kaolinite (001) surface shows only a slight enhancement of the hydrogen-bonding of water compared to solvated Gb1 without any surface present. The three complexes, Gb1-Na^+-MMT (001), Gb1-Ca^{2+}-MMT (001), and Na^+-birnessite show suppression of water hydrogen-bonding compared with the solvated Gb1 system without a surface present. These Gb1-Na^+-MMT (001), Gb1-Ca^{2+}-

MMT (001), and Gb1-Na^+-birnessite complexes have solvated cations that can disrupt water hydrogen-bonding. Compared to the Gb1-Na^+-MMT (001) and Gb1-Ca^{2+}-MMT (001) systems with nearly equal water hydrogen-bonding profiles, the Gb1-Na^+-birnessite complex slightly suppresses the water hydrogen-bonding network more. This could be one reason why the Na^+-birnessite system is more disruptive to the Gb1 folded structure compared with the other surfaces.

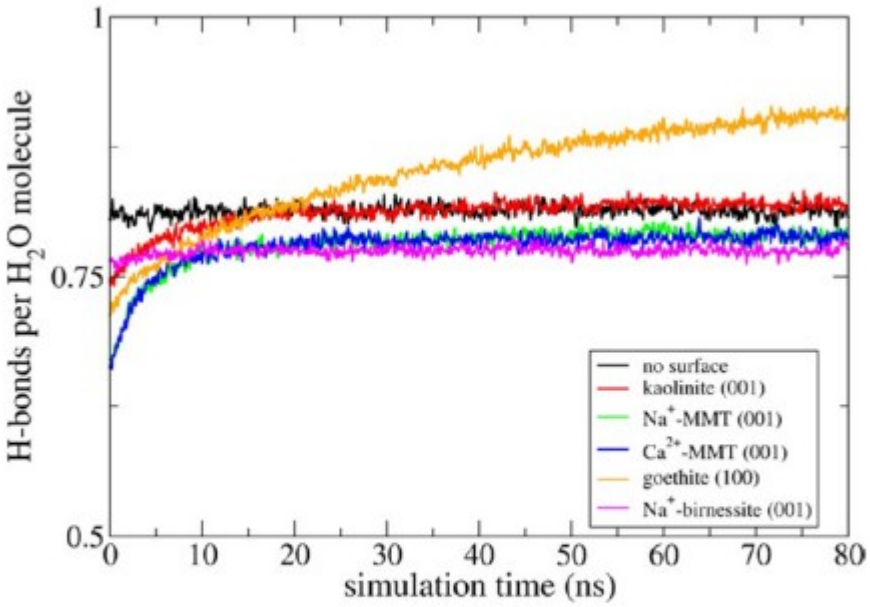

Figure 12. Normalized H_2O H-bond count for the five solvated Gb1 mineral complexes and solvated Gb1 with no surface, starting from 0 ns after equilibration.

To further explore the water network, we compared the water tetrahedral order parameter for the five Gb1 mineral surface complexes (Figure 13). Similar features are found with each of the five Gb1 mineral surface complexes and the solvated Gb1 without a mineral surface: a peak feature at ~0.7–0.75 and a shoulder peak feature at ~0.55. The first feature at ~0.75 is most pronounced for the solvated Gb1 system over the goethite (100) surface, indicating that the goethite surface possibly induces a more orderly structure to water over the surface compared with the other systems. This is consistent with the increasing hydrogen bonding network of the Gb1-goethite (100) system shown in Figure 12. The baseline solvated Gb1 without a mineral surface has the second most prominent peak around ~0.7, followed closely by the Gb1-kaolinite (001) complex. The Gb1-Na^+-MMT(001), Gb1-Ca^{2+}-MMT (001), and Gb1-Na^+-birnessite (001) complex systems shows the most decrease in the ~0.7 peak. The shoulder peak is most pronounced in these three systems, indicating a more disorderly water structure. These observations are in line with the hydrogen-bonding data that show the most hydrogen-bonding with the Gb1-goethite (100) complex, a hydrogen-bonding

network of the Gb1-kaolinite (001) system almost on par with the solvated Gb1 system without a surface, and the similar hydrogen-bonding suppression with respect to the surfaceless solvated Gb1 system for the Gb1-Na^+/Ca^{2+}-MMT (001) complexes and Gb1-Na^+-birnessite (001) complex (see Figure 12).

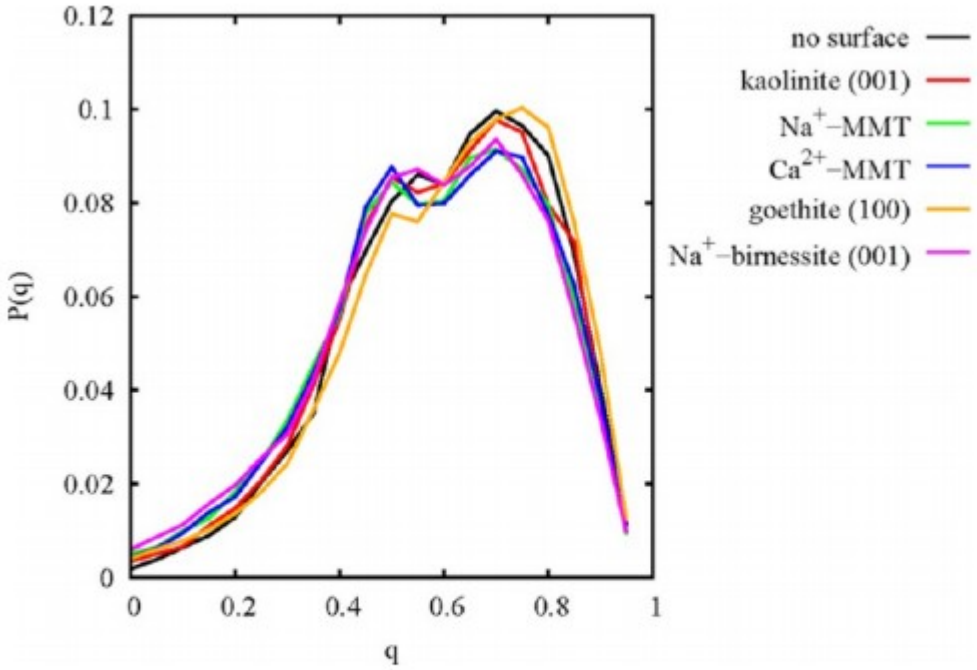

Figure 13. Tetrahedral order parameter of the water molecules for the five solvated Gb1 mineral complex systems and solvated Gb1 with no surface.

Figure 14 shows the density of water as a function of the *z*-axis, normal to mineral surfaces. The water density at the basal surface of Na^+-birnessite is the highest of the five systems (~4 g/cm^3), and there is a small depression in the H_2O density between the first surface layer and the second surface layer (~1.5 g/cm^3). The goethite (100) surface has ~3 g/cm^3 peak H_2O density right at the surface, a depression above the first peak, and second substantial ~2 g/cm^3 peak H_2O density. The kaolinite (001) surface also has a peak H_2O density at the surface of around 3 g/cm^3, but, unlike the birnessite (001) and goethite (100) systems, the kaolinite (001) system does not have a deep trough in the water density above the peak density region above the surface. The least surface peak water density above a surface is observed for the two MMT basal surface systems considered here. For both Na^+ and Ca^{2+}-MMT, the peak water density just above the surface is ~2 g/cm^3 with a negligible trough above this surface water layer. The peak surface water densities in these systems may indicate the degree of surface hydration that needs to be displaced for full contact of the protein system with the surfaces.

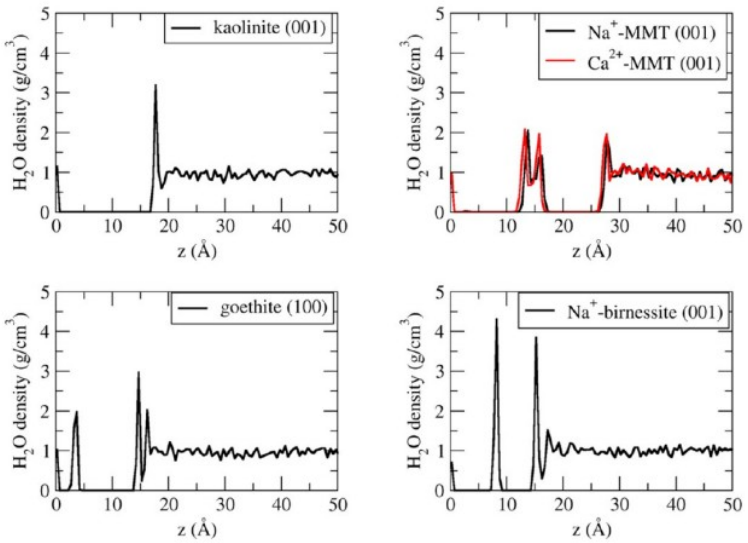

Figure 14. H_2O density as a function of the *z* coordinate normal to the mineral slab surface, starting from the bottom *xy* plane of the simulation cell, for the five Gb1 mineral complexes studied here.

3.5.3 Solvated Gb1 Mineral Interaction

Figure 15 shows color maps depicting the distance each Gb1 residue is from the five mineral surfaces as a function of simulation time. Note that in the case of Na^+-MMT, Ca^{2+}-MMT, and Na^+-birnessite, the counter cations compete with mineral surface sites as well as counter the net negative charge of the Gb1 protein. Kaolinite, on the other hand, is a neutral polar surface with no cations, and, therefore, can have a more intimate contact with the Gb1 protein (as shown in Figure 14). For goethite (100), Gb1 must compete with water double-layer. In the case of Na^+-birnessite, the Na^+ cations are held relatively close to the birnessite, and Gb1 GLU and ASP residues are attracted to these cation sites on the surface. Interestingly, ALA24, a hydrophobic residue is surprisingly close to the surfaces. This residue is in the small fragment of the distorted α-helix closest to the surface. ALA24 has negatively charged (under pH 7) carboxylate-bearing ASP22 and GLU41 on either side, which are attracted to positively charged ions on the surface and may aid in pinning down ALA24 to the surface.

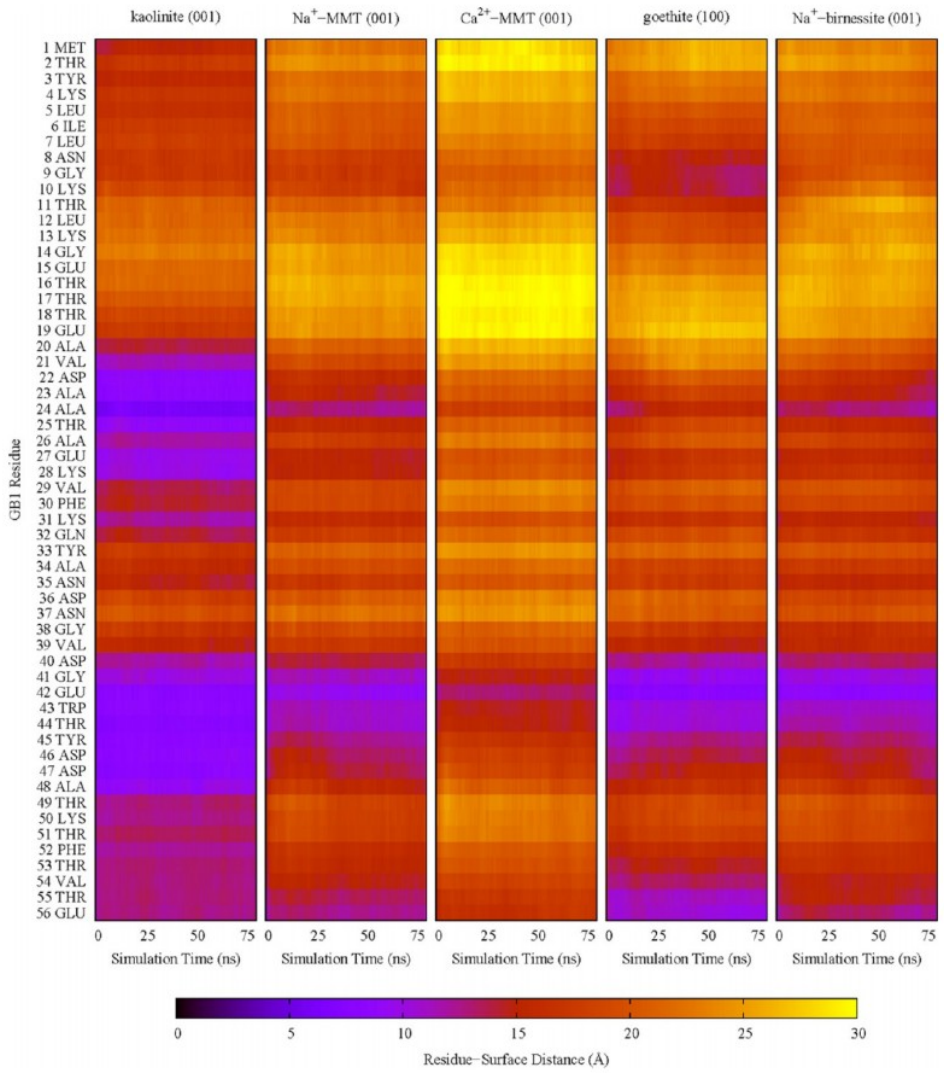

Figure 15. Heat maps for Gb1 residue-mineral surface distances as a function of simulation time. Note that the distance is measured from the maximum z value of the mineral surface to the z value of the backbone α-carbon of each residue.

To further explore the interaction between the Gb1 and the five mineral surfaces and to estimate the free energy of binding, metadynamics simulations with the center-of-mass distance collective variable were conducted. In each of the mineral cases, depletion of the water molecules between Gb1 and the mineral surface lead to a minimum free energy profile with the Gb1 closer to the mineral surface. In the case where counter cations could be readily solvated and could diffuse away from the surface [notably Na^+-MMT (001) and Ca^{2+}-MMT (001) and, to a lesser extent, Na^+-birnessite (001)], a complex free energy profile emerged due to diffusion leading to a graded layer concentration of counter cations at these mineral surfaces. The potential of mean force (PMF) free energy plots for the Gb1 center of mass (COM) distance from the surface collective variable are shown in Figure 16 and the Gb1 free energies of adsorption to the five mineral surfaces of interest are summarized in Table 2.

Table 2. Gb1 Free Energies of Adsorption to the Five Mineral Surfaces of Interest in This Work

surface	F_{ads} (kcal/mol)
kaolinite (001)	−96
Na^+-MMT (001)	−121
Ca^{2+}-MMT (001)	−72
goethite (100)	−166
Na^+-birnessite (001)	−104

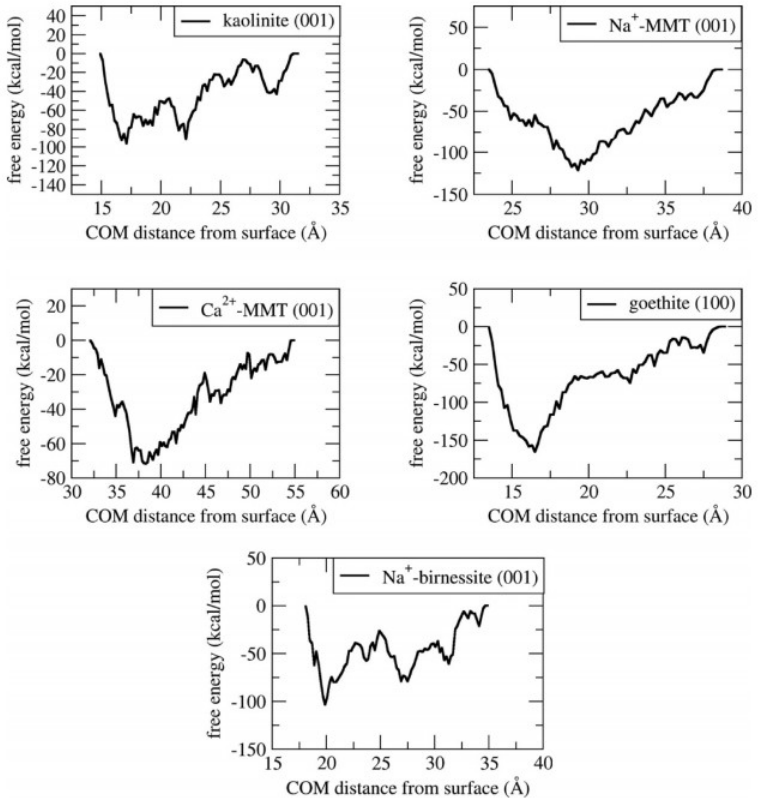

Figure 16. Metadynamics potential of mean force (PMF) plots for collective variable of the Gb1 center of mass (COM) distance from the surface.

The free energy of Gb1 binding magnitude was largest for the goethite (100) surface (−166 kcal/mol). Though protein is a subset of NOM and not completely comparable to NOM, this result is in line with the strong Fe^{3+}-carboxylate binding as indicated by the DRIFT spectra analysis presented in the paper by Chorover and Amistadi for negatively charged carboxylate-bearing NOM.(19) Gb1 binding to the Na^+-birnessite (001) surface is lower in magnitude than that of the goethite (100) surface by 62 kcal/mol (−104 kcal/mol). According to the work by Chorover and Amistadi,(19) NOM is not retained by birnessite as much as it is by goethite, but it is possible that changing the chemical characteristics of the NOM functional groups may cause ready desorption of NOM material. According to the AFM and FTIR

work of Naidja et al.,(20) protein tyrosinase (which may be able to mitigate redox oxidative damage with its multicopper active site) is readily adsorbed to birnessite, but the free energy of adsorption of tyrosinase was not determined.

Over kaolinite, the free energy profile of Gb1 adsorption shows a local minimum that is only 5 kcal/mol above the global minimum and 5 Å higher than the position of the global minimum above the surface of kaolinite. The barrier to move from this local minimum to the global minimum close to the kaolinite surface is 44 kcal/mol, requiring the displacement of the surface water layer. Gb1 binding to the gibbsite side of the kaolinite (001) surface is less favorable than that of the goethite(100) surface by 70 kcal/mol (−96 kcal/mol). Over birnessite, we also see multiple free energy minima in the Gb1 adsorption. Like the kaolinite case, this could be due to an energy requirement for displacing the surface water layers. This also could be due to further changes in the Gb1 structure over the birnessite surface.

The Gb1 free energy of binding to the Na^+-MMT (001) and Ca^{2+}-MMT (001) surfaces is less than that of goethite (100) (−121 kcal/mol and −72 kcal/mol, respectively). Gb1 over the MMT surfaces shows considerable tilting with the depletion of surface-adsorbed cations; the LYS10 and LYS13 end comes down toward the negative MMT surface (which becomes increasingly unscreened due to depletion of surface cations), and the dipole-surface normal angle becomes more acute at the free energy minimum in the metadynamics. The binding energy of Gb1 to the Na^+-MMT (001) is much greater than that of Ca^{2+}-MMT (001) and is greater than that of both kaolinite (001) and Na^+-birnessite (001). As the metadynamics progresses, Gb1 is better able to penetrate the depleting Na^+ ion layer over the Na^+-MMT (001) surface compared to Gb1 at the Ca^{2+} layer over the Ca^{2+}-MMT (001) surface. Moreover, the Na^+ cation vertical layer tends to surround Gb1 at the Na^+-MMT (001) surface. The Na^+ may act to screen the overall negative charge of the carboxylate groups, and the Na^+ cations at the surface bind carboxylate groups to the surface. Thus, both the carboxylate groups and the ammonium groups of Gb1 are attracted to the Na^+-MMT (001) surface with a vertically broad, depleting Na^+ surface layer. Importantly, the resulting desorbed structures retain the folded Gb1 native structure for all Gb1-surface complex systems except for the Gb1-Na^+-birnessite (001) complex system. The desorbed Gb1 structure in the Na^+-birnessite (001) case has an even greater overall RMSD deviation (as high as 4.780 Å) compared with the adsorbed Gb1 structure in the conventional molecular dynamics simulation.

3.5.4 Comparison of Simulation versus Recent Experimental Data

An experimental investigation of Gb1 behavior at kaolinite and birnessite surfaces has recently been reported by Reardon et al.(70) For reasons of experimental tractability, the background electrolyte concentration in these experiments had to be set at 5 mMol of Na^+ and the time scale of observation was 72 h, compared to the assumption of complete Na^+

saturation in the simulations. Moreover, the hexagonal, very low Mn^{3+} content “acid birnessite” of these experiments is likely to have Mn vacancies, which are akin to edge sites with attached protons at low pH. Despite these differences in conditions and birnessite structure, our simulation results, which assume a triclinic lattice structure with hexagonally patterned Mn and O atom positions, indicate potential reactivity of Gb1 over birnessite systems via disruption of the folded structure rendering the protein vulnerable to oxidative or hydrolysis attack. In line with the simulations reported here, two-dimensional NMR did not detect any fragmentation of Gb1 after contact with kaolinite surfaces, but showed some response of the Gb1 molecule to the birnessite surface at pH 7, albeit after an exposure time of 72 h. We conclude from these observations that background electrolyte concentration and the nature of counterions may have a yet underappreciated role in modulating the behavior and physical integrity of large biomolecules as they come in contact with mineral surfaces.

3.6 Summary

We have performed conventional and metadynamics molecular dynamics simulations of model protein Gb1 interacting with mineral surfaces of five common soil minerals, kaolinite (001), Na^+-montmorillonite (001), Ca^{2+}-montmorillonite (001), goethite (100), and Na^+-birnessite (001), to determine the characteristics and degree of protein adsorption on these mineral surfaces. The conventional MD simulations show that all surfaces studied do not have a profound impact on the Gb1 folded structure except for the Na^+-birnessite (001). The RMSD goes as follows: Na^+-birnessite (001) > Ca^{2+}-montmorillonite (001) > kaolinite (001) > goethite (100) > Na^+-montmorillonite (001). The Na^+-birnessite (001) surface appears to flatten the Gb1 structure and cause some unfolding of the β-sheet structure around the turn with a positively charged LYS 10 and the α-helix around ALA24. This may be due to a unique water structure above the birnessite (001) surface, high Na^+ charge held closely to the birnessite (001) surface, and the unique nonbonding interactions of the birnessite system. In contrast, Na^+-montmorillonite has a high ionic concentration/strength of Na^+ at the MMT surface, which may stabilize the structure to a degree that is within 1 Å RMSD of the solution-state NMR-determined structure. The other three surfaces have positive charges [Ca^{2+} in the case of Ca^{2+}-MMT, surface protons in the case of the aluminum side of kaolinite, and the Fe^{3+} and hydroxyl termination of the goethite (100) with labile water molecules] that are either closely held to the surface or terminate the surface, which lead to increased tethering of the carboxylate functional groups to the surface and, therefore, lead to slight strain on the Gb1 structure as seen in the RMSD analysis.

From the metadynamics simulations, the adsorption free energies were calculated. The trend in the adsorption free energies is goethite (100) > Na^+-montmorillonite (001) > Na^+-birnessite (001) > kaolinite (001) > Ca^{2+}-

montmorillonite (001). In contrast to the trend in the RMSD, the Gb1-Na^+-montmorillonite (001) complex binding is much more stable than that for Gb1-Ca^+-montmorillonite (001), despite the RMSD deviation of Gb1 over Ca^+-montmorillonite (001) being greater than that for Gb1 over Na^+-montmorillonite (001). This could be due to a higher ionic strength of Na^+ vertical layer encompassing the Gb1 over the MMT basal surface in contrast to the Ca^{2+} vertical layer, which tends to stay closer to the clay surface and only partially surrounds the Gb1. Though the free energies of adsorption for Gb1- Na^+-birnessite (001) and Gb1- kaolinite (001) are close, the RMSD for Gb1 is greater over Na^+-birnessite (001) compared to that of Gb1- kaolinite (001). Contrasting transition metal oxide Gb1 binding free energies, Gb1 adsorption to goethite (100) is much stronger than the birnessite (001) surface due to the zwitterionic nature of the goethite surface, including Fe^{3+} sites available for chemisorption of protein carboxylate side groups. However, the goethite (100) surface preserves the Gb1 structure according to the Gb1 RMSD of the goethite simulations. Though quantum mechanical calculations are needed to study possible hydrolysis and oxidation of the protein by the transition metal surfaces, the insight gained by classical MD simulations show an opportunity for significant protein structural changes over birnessite as indicated by the calculated high RMSD and binding affinity (i.e., potential residence time at catalytic sites on the surface). With active out-of-plane Mn catalytic sites of birnessite being more plentiful at low pH, the disturbed structure of Gb1 over low Mn vacancy birnessites will have more opportunity for permanent structure-changing reactions at low pH compared with neutral pH. Over birnessites with high Mn vacancies (low Mn^{3+}), the vacancies may be compared to oxygen edge sites that are attractive to proton adsorption, and catalytic reactions of the protein at these edge-like structures can occur (as shown by recent experiments by Reardon et al.(70)). Moreover, edge sites of the layered minerals birnessite, kaolinite, and MMT may show higher binding and more potential reactivity toward protein and will be the subject of future studies.

4 Conclusions

The work presented here reveals valuable details regarding the degree and modes of protein-mineral interactions for a variety of mineral surfaces found in soil systems and sheds light on possible mechanisms for the stabilization or decomposition of proteinaceous soil organic matter. Moreover, this knowledge contributes to an eventual understanding of how soil microorganisms may evolve to “design” exoenzymes that function in soil environments with numerous and diverse mineral interfaces. Molecular dynamics simulations, conventional and those using enhanced sampling methods such as metadynamics, provide mechanistic detail that is otherwise difficult to obtain or determine via experimental means. While the necessary level of expertise to perform molecular dynamics simulations is often not available to teams of experimental/empirical researchers, emphasis on joint

modeling/experimental work is demonstratively an encouraged strategy in the study of complex systems such as soils.

Acknowledgments

We thank Dr. Niri Govind for his insightful discussions regarding the manuscript. The research is part of the “Understanding Molecular-Scale Complexity and Interactions of Soil Organic Matter” Intramural Project at EMSL, a DOE Office of Science User Facility sponsored by the Office of Biological and Environmental Research and located at Pacific Northwest National Laboratory. PNNL is operated by Battelle for the U.S. DOE under Contract DE-AC05-76RL01830.

References

(1) Schmidt, M. W. I.; Torn, M. S.; Abiven, S.; Dittmar, T.; Guggenberger, G.; Janssens, I. A.; Kleber, M.; Kogel-Knabner, I.; Lehmann, J.; Manning, D. A. C.; Nannipieri, P.; Rasse, D. P.; Weiner, S.; Trumbore, S. E. Persistence of soil organic matter as an ecosystem property. Nature 2011, 478, 49−56.

(2) Stockmann, U.; Adams, M. A.; Crawford, J. W.; Field, D. J.; Henakaarchchi, N.; Jenkins, M.; Minasny, B.; McBratney, A. B.; de Remy de Courcelles, V.; Singh, K.; Wheeler, I.; Abbott, L.; Angers, D. A.; Baldock, J.; Bird, M.; Brookes, P. C.; Chenu, C.; Jastrow, J. D.; Lal, R.; Lehmann, J.; O’Donnell, A. G.; Parton, W. J.; Whitehead, D.; Zimmerman, M. The knowns, known unknowns and unknowns of sequestration of soil organic carbon. Agric., Ecosyst. Environ. 2013, 164, 80−99.

(3) von Lützow, M.; Kö gel-Knabner, I.; Ekschmitt, K.; Matzner, E.; Guggenberger, G.; Marschner, B.; Flessa, H. Stabilization of organic matter in temperate soils: mechanisms and their relevance under different soil conditions - a review. Eur. J. Soil Sci. 2006, 57, 426−445.

(4) Qafoku, N. Climate-change effects on soils: Accelerated weathering, soil carbon and elemental cycling. In Advances in Agronomy; Sparks, D. L., Ed.; Elsevier: Amsterdam, Netherlands, 2015; pp 111−172.

(5) Zimmerman, A. R.; Ahn, M.-Y. Organo-Mineral-Enzyme Interaction and Soil Enzyme Activity. In Soil Enzymology, Soil Biology; Shukla, G., Varma, A., Eds.; Springer-Verlag: Berlin, Heidelberg, 2011; Vol. 22.

(6) Naidja, A.; Huang, P. M.; Bollag, J.-M. Enzyme-Clay Interactions and their Impact on Transformations of Natural and Anthropogenic Organic Compounds in Soil. J. Environ. Quality 2000, 29, 677−691.

(7) van Loosdrecht, M. C.; Lyklema, J.; Norde, W.; Zehnder, A. J. Influence of interfaces on microbial activity. Microbiol. Mol. Biol. Rev. 1990, 54, 75−87.

(8) Russo, F.; Johnson, C. J.; Johnson, C. J.; McKenzie, D.; Aiken, J. M.; Pedersen, J. A. Pathogenic prion protein is degraded by a manganese oxide mineral found in soils. J. Gen. Virol. 2009, 90, 275− 280.

(9) Liu, X.; Eusterhues, K.; Thieme, J.; Ciobota, V.; Hö schen, C.; Mueller, C. W.; Kü sel, K.; Kö gel-Knabner, I.; Rö sch, P.; Popp, J.; Totsche, K. U. STXM and NanoSIMS Investigation on EPS Fractions before and after Adsorption to Geothite. Environ. Sci. Technol. 2013, 47, 3158−3166.

(10) Olsson, R.; Giesler, R.; Loring, J. S.; Persson, P. Enzymatic Hydrolysis of Organic Phosphates Adsorbed on Mineral Surfaces. Environ. Sci. Technol. 2012, 46, 285−291.

(11) Rao, M. A.; Violante, A.; Gianfreda, L. Interaction of acid phosphatase with clays, organic molecules and organo-mineral complexes: kinetics and stability. Soil Biol. Biochem. 2000, 32, 1007− 1014.

(12) Naidja, A.; Huang, P. M. Aspartic acid interaction with Camontmorillonite adsorption, desorption and thermal stability. Appl. Clay Sci. 1994, 9, 265−281.

(13) Naidja, A.; Huang, P. M. Significance of the Henri-MichaelisMenten theory in abiotic catalysis: catechol oxidation by δ-MnO2. Surf. Sci. 2002, 506, L243−L249.

(14) Naidja, A.; Huang, P. M.; Bollag, J.-M. Activity of tyrosinase immobilized on hydroxyaluminum-montmorillonite complexes. J. Mol. Catal. A: Chem. 1997, 115, 305−316.

(15) Spence, A.; Kelleher, B. P. FT-IR spectroscopic analysis of kaolinite-microbial interactions. Vib. Spectrosc. 2012, 61, 151−155.

(16) Rigou, P.; Rezaei, H.; Grosclaude, J.; Staunton, S.; Quiquampoix, H. Fate of Prions in Soil: Adsorption and Extraction by Electroelution of recombinant Ovine Prion Protein from Montmorillonite and National Soils. Environ. Sci. Technol. 2006, 40, 1497−1503.

(17) Lepoitevin, M.; Jaber, M.; Guegan, R.; Janot, J.-M.; Dejardin, P.;´ Henn, F.; Balme, S. BSA and lysozyme adsorption on homoionic montmorillonite: Influence of the interlayer cation. Appl. Clay Sci. 2014, 95, 396−402.

(18) Assifaoui, A.; Huault, L.; Maissiat, C.; Roullier-Gall, C.; Jeandet, P.; Hirschinger, J.; Raya, J.; Jaber, M.; Lambert, J.-F.; Cayot, P.; Gougeon, R. D.; Loupiac, C. Structural Studies of adsorbed protein (betalactoglobulin) on natural clay (montmorillonite). RSC Adv. 2014, 4, 61096−61103.

(19) Chorover, J.; Amistadi, M. K. Reaction of forest floor organic matter at goethite birnessite and smectite surfaces. Geochim. Cosmochim. Acta 2001, 65, 95−109.

(20) Naidja, A.; Liu, C.; Huang, P. M. Formation of ProteinBirnessite Complex: XRD, FTIR, and AFM Analysis. J. Colloid Interface Sci. 2002, 251, 46−56.

(21) Kolman, K.; Makowski, M. M.; Golriz, A. A.; Kappl, M.; Pigłowski, J.; Butt, H.-J.; Kiersnowski, A. Adsorption, Aggregation, and Desorption of Proteins on Smectite Particles. Langmuir 2014, 30, 11650−11659.

(22) Johnston, C. T.; Premachandra, G. S.; Szabo, T.; Lok, J.; Schoonheydt, R. A. Interaction of Biological Molecules with Clay Minerals: A Combined Spectroscopic and Soption Study of Lysozyme on Saponite. Langmuir 2012, 28, 611−619.

(23) Servagent-Noinville, S.; Revault, M.; Quiquampoix, H.; Baron, M.-H. Conformational Changes of Bovine Serum Albumin Induced by Adsorption on different clay Surfaces: FTIR Analysis. J. Colloid Interface Sci. 2000, 221, 273−283.

(24) Madliger, M.; Gasser, C. A.; Schwarzenbach, R. P.; Sander, M. Adsorption of Transgenic Insecticidal Cry1Ab Protein to Silica Particles. Effects on Transport and Bioactivity. Environ. Sci. Technol. 2011, 45, 4377−4384.

(25) Barral, S.; Villa-García, M. A.; Rendueles, M.; Díaz, M. Interactions between whey proteins and kaolinite surfaces. Acta Mater. 2008, 56, 2784−2790.

(26) Duarte-Silva, R.; Villa-García, M. A.; Rendueles, M.; Díaz, M. Structural, textural and protein adsorption properties of kaolinite and surface modified kaolinite adsorbents. Appl. Clay Sci. 2014, 90, 73−80.

(27) Cengiz, S.; Çavas, L.; Yurdakoc¸ , K. Bentonite and sepiolite as¸ supporting media: Immobilization of catalase. Appl. Clay Sci. 2012, 65−66, 114−120.

(28) Kim, H. J.; Suma, Y.; Lee, S. H.; Kim, J.-A.; Kim, H. S. Immobilization of horseradish peroxidase onto clay minerals using soil organic matter for phenol removal. J. Mol. Catal. B: Enzym. 2012, 83, 8−15.

(29) Sedaghat, M. E.; Ghiaci, M.; Aghaei, H.; Soleimanian-Zad, S. Enzyme immobilization. Part 3 Immobilizaation of alpha-amylase on Na-bentonite and modified bentonite. Appl. Clay Sci. 2009, 46, 125− 130.

(30) Reshmi, R.; Sugunan, S. Superior activities of lipase immobilized on pure an dhydrophobic clay supports: Caracterization and catalytic activity studies. J. Mol. Catal. B: Enzym. 2013, 97, 36−44.

(31) Sutton, R.; Sposito, G.; Diallo, M. S.; Schulten, H.-R. Molecular simulation of a model of dissolved organic matter. Environ. Toxicol. Chem. 2005, 24, 1902−1911.

(32) Sutton, R.; Sposito, G. Molecular simulation of humic substance-Ca-montmorillonite complexes. Geochim. Cosmochim. Acta 2006, 70, 3566−3581.

(33) Iskrenova-Tchoukova, E.; Kalinichev, A. G.; Kirkpatrick, R. J. Metal Cation Complexation with Natural Organic Matter in Aqueous Solutions: Molecular Dynamics Simulations and Potentials of Mean Force. Langmuir 2010, 26, 15909−15919.

(34) Kalinichev, A. G.; Iskrenova-Tchoukova, E.; Ahn, W.-Y.; Clark, M. M.; Kirkpatrick, R. J. Effects of Ca2+ on supramolecular aggregation of natural

organic matter in aqueous solutions: A comparison of molecular modeling approaches. Geoderma 2011, 169, 27−32.

(35) Swadling, J. B.; Coveney, P. V.; Greenwell, H. C. Clay Minerals Mediate Folding and Regioselective Interactions of RNA: A LargeScale Atomistic Simulation Study. J. Am. Chem. Soc. 2010, 132, 13750−13764.

(36) Swadling, J. B.; Suter, J. L.; Greenwell, H. C.; Coveney, P. V. Influence of Surface Chemistry and Charge on Mineral-RNA Interactions. Langmuir 2013, 29, 1573−1583.

(37) Swadling, J. B.; Wright, D. W.; Suter, J. L.; Coveney, P. V. Structure, Dynamics, and Function of the Hammerhead Ribozyme in Bulk Water and at a Clay Mineral Surface from Replica Exchange Molecular Dynamics. Langmuir 2015, 31, 2493−2501.

(38) Thyveetil, M.-A.; Coveney, P. V.; Greenwell, H. C.; Suter, J. L. Computer Simulation Study of the Structrural Stability and Materials Properties of DNA-Intercalated Layered Double Hydroxides. J. Am. Chem. Soc. 2008, 130, 4742−4756.

(39) Gregoire, B.; Erastova, V.; Geatches, D. L.; Clark, S. J.;´ Greenwell, H. C.; Fraser, D. G. Insights into the behaviour of biomolecules on the early Earth: The concentration of aspartate by layered double hydroxide minerals. Geochim. Cosmochim. Acta 2016, 176, 239−258.

(40) Kubiak-Ossowska, K.; Mulheran, P. A. Mechanism of Hen Egg White Lysozyme Adsorption on a Charged Solid Surface. Langmuir 2010, 26, 15954−15965.

(41) Kubiak-Ossowska, K.; Mulheran, P. A. What Governs Protein Adsorption and Immobilization at a Charged Solid Surface? Langmuir 2010, 26, 7690−7694.

(42) Kubiak-Ossowska, K.; Mulheran, P. A.; Nowak, W. fibronectin Module FNIII9 Adsorption at Contrasting Solid Model Surfaces Studied by Atomistic Molecular Dynamics. J. Phys. Chem. B 2014, 118, 9900−9908.

(43) Zhao, D.; Peng, C.; Zhou, J. Lipase adsorption on different nanomaterials: a multi-scale simulation study. Phys. Chem. Chem. Phys. 2015, 17, 840−850.

(44) Gronenborn, A. M.; Filpula, D. R.; Essig, N. Z.; Achari, A.; Whitlow, M.; Wingfield, P. T.; Clore, G. M. A Novel, Highly Stable Fold of the Immunogloblin Binding Domain of Streptococcal Protein G. Science 1991, 253, 657−661.

(45) Frericks Schmidt, H. L.; Sperling, L. J.; Gao, Y. G.; Wylie, B. J.; Boettcher, J. M.; Wilson, S. R.; Rienstra, C. M. Crystal Polymorphism of Protein GB1 Examined by Solid-State NMR Spectroscopy and Xray Diffraction. J. Phys. Chem. B 2007, 111, 14362−14369.

(46) Wieder, W. R.; Allison, S. D.; Davidson, E. A.; Georgiou, K.; Hararuk, O.; He, Y.; Hopkins, F.; Luo, Y.; Smith, M. J.; Sulman, B.; Todd-Brown, K.; Wang,

Y.-P.; Xia, J.; Xu, X. Explicitly representing soil microbial processes in Earth system models. Global Biogeochemical Cycles 2015, 29, 1782−1800.

(47) Bish, D. L.; Von Dreele, R. B. Rietveld refinement of nonhydrogen atomic positions in kaolinite. Clays Clay Miner. 1989, 37, 289−296.

(48) Bish, D. L. Rietveld refinement of non-hydrogen atomic positions in kaolinite. Clays Clay Miner. 1993, 41, 738−744.

(49) Viani, A.; Gualtieri, A. F.; Artioli, G. The nature of disorder in montmorillonite by simulation of X-ray powder patterns. Am. Mineral. 2002, 87, 966−975.

(50) Yang, H.; Lu, R.; Downs, R. T.; Costin, G. Goethite, αFeO(OH), from single−crystal data. Acta Crystallogr., Sect. E: Struct. Rep. Online 2006, E62, i250−i252.

(51) Lopano, C. L.; Heaney, P. J.; Post, J. E.; Hanson, J.; Komarneni, S. Time-resolved structural analysis of K- and Ba-exchange reactions with synthetic Na-birnessite using synchrotron X-ray diffraction. Am. Mineral. 2007, 92, 380−387.

(52) Cygan, R. T.; Liang, J.-J.; Kalinichev, A. G. Molecular models of hydroxide, oxyhydroxide, and clay phases and the development of a general force field. J. Phys. Chem. B 2004, 108, 1255−1266.

(53) Berendsen, H. J. C.; Grigera, J. R.; Straatsma, T. P. The Missing Term in Effective Pair Potentials. J. Phys. Chem. 1987, 91, 6269−6271.

(54) Materials Studio, Release 5.5.3; Accelrys Software, Inc.: San Diego, 2010.

(55) Liu, J.; Liao, C.; Zhou, J. Multiscale Simulations of Protein GB1 Adsorbed on Charged Self-Assembled Monolayers. Langmuir 2013, 29, 11366−11374.

(56) Martínez, L.; Andrade, R.; Birgin, E. G.; Martínez, J. M. Packmol: A package for building initial configurations for molecular dynamics simulations. J. Comput. Chem. 2009, 30, 2157−2164 http:// www.ime.unicamp.br/~martinez/packmol/.

(57) Plimpton, S. Fast Parallel Algorithms for Short-Range Molecular Dynamics. J. Comput. Phys. 1995, 117, 1−19 http://lammps.sandia. gov.

(58) Case, D. A.; Babin, V.; Berryman, J. T.; Betz, R. M.; Cai, Q.; Cerutti, D. S.; Cheatham, T. E., III; Darden, T. A.; Duke, R. E.; Gohlke, H.; Goetz, A. W.; Gusarov, S.; Homeyer, N.; Janowski, P.; Kaus, J.; Kolossvary, I.; Kovalenko, A.; Lee, T. S.; LeGrand, S.; Luchko,´ T.; Luo, R.; Madej, B.; Merz, K. M.; Paesani, F.; Roe, D. R.; Roitberg, A.; Sagui, C.; Salomon-Ferrer, R.; Seabra, G.; Simmerling, C. L.; Smith, W.; Swails, J.; Walker, R. C.; Wang, J.; Wolf, R. M.; Wu, X.; Kollman, P. A. AMBER 14; University of California: San Francisco, 2014.

(59) Andersen, A. Molecular modeling of phases of manganese oxides including hydrous birnessite: development of a new classical potential. In preparation.

(60) Kerisit, S. Water structure at hematite-water interfaces. Geochim. Cosmochim. Acta 2011, 75, 2043−2061.

(61) Humphrey, W.; Dalke, A.; Schulten, K. J. Mol. Graphics 1996, 14, 33−38 http://www.ks.uiuc.edu/Research/vmd/.

(62) Fiorin, G.; Klein, M. L.; Henin, J. Using collective variables to´ drive molecular dynamics simulations. Mol. Phys. 2013, 111, 3345− 3362.

(63) Gupta, V.; Miller, J. D. Surface force measurements at the basal plances of ordered kaolinite particles. J. Colloid Interface Sci. 2010, 344, 362−371.

(64) Wei, T.; Carignano, M. A.; Szleifer, I. Molecular Dynamics Simulation of Lysozyme Adsorption/Desorption on Hydrophobic Surfaces. J. Phys. Chem. B 2012, 116, 10189−10194.

(65) Yu, G.; Liu, J.; Zhou, J. Mesoscopic Coarse-Grained Simulations of Lysozyme Adsorption. J. Phys. Chem. B 2014, 118, 4451−4460.

(66) De Cristofaro, A.; Violante, A. Effect of hydroxy-aluminum species on the sorption and interlayering of albumin onto montmorillonite. Appl. Clay Sci. 2001, 19, 59−67.

(67) Boily, J.-F. Water Structure and Hydrogen Bonding at Goethite/ Water Interfaces: Implications for Proton Affinities. J. Phys. Chem. C 2012, 116, 4714−4724.

(68) Lanson, B.; Drits, V. A.; Silvester, E.; Manceau, A. Structure of H-exchanged hexagonal birnessite and its mechanism of formation from Na-rich monoclinic buserite at low pH. Am. Mineral. 2000, 85, 826−838.

(69) Villalobos, M.; Toner, B.; Bargar, J. R.; Sposito, G. Characterization of the manganese oxide produced by pseudomonas putida strain MnB1. Geochim. Cosmochim. Acta 2003, 67, 2649−2662.

(70) Reardon, P. N.; Chacon, S. S.; Walter, E. D.; Washton, N. M.; Kleber, M. Abiotic protein fragmentation by manganese oxide: a mechanism to supply soil biota with oligopeptides. Environ. Sci. Technol. 2016, 50, 3486.